RSC Advances

ROYAL SOCIETY OF CHEMISTRY

www.rsc.org/advances

Cite this: DOI: 10.1039/c0xx00000x

www.rsc.org/xxxxxx

ARTICLE TYPE

Extension of high-order harmonic generation cutoff via control of chirped laser pulses in the vicinity of metal nanostructure media

H. Hekmatara*[a]

Received (in XXX, XXX) Xth XXXXXXXXX 20XX, Accepted Xth XXXXXXXXX 20XX

DOI: 10.1039/b000000x

We use the local field enhancement induced by resonant plasmons within a metallic nanostructure to generate high-order harmonic in an 800-nm femtosecond laser pulse. Numerical results show that, with chirping inhomogeneous field, the cutoff position of the HHG spectra is extended. By using suitable parameters, laser chirp and inhomogeneity parameters, only the short trajectories are selected. As a result, obtained wide continuum spectrum shows little modulation can be led to the generation of short single attosecond pulses. To better understand the physical mechanism of this behavior, we analyze the time-frequency characteristics of HHG and perform semi-classical simulations.

Introduction

The interaction of nanostructures with laser pulse is now fascinating topic to research[1,2]. Plasmonic nanostructures suggest singular feasibilities for intensifying linear and nonlinear optical processes[3-8]. Recent experiments using a combination of plasmonic nanostructures and rare gases exhibited that the high-order harmonic can be generated[9,10]. The process known as high-order harmonic generation (HHG), in which an atomic or molecular system is subjected to an intense laser field, high-order harmonics of the driving field are generated.

This process can be physically understood in terms of the semi-classical three-step model[11]: the electron first tunnels through the barrier formed by the Coulomb potential and the laser field, then it oscillates almost freely in the laser field, and finally it may return to the ground state by recombining with the parent ion. During the recombination, a photon with energy equal to the ionization potential plus the kinetic energy of the recombining electron is emitted. The harmonic cutoff of the gases can be more extended by using the field, locally enhanced due to the coupling of a laser pulse with nanostructures[9,10]. Field enhancement is related to the collective motion of free electrons limited in narrowly localized regions, similar to that observed in colloidal nanoparticles exposed to an external electromagnetic field[9,12]. For a typical geometry of nanostructure, the value of field enhancement can be estimated by solving Maxwell's equations numerically[13]. In addition, the geometrical shape of the metallic nanostructure largely affects the field enhancement[9].

Kim et al.[9], reported in the vicinity of the bow-tie-shaped nanostructure with a 20-nm gap, the driving laser field is increased to three orders of magnitude between the vertices. The enhanced intensity was large enough to produce harmonics as high as the 17th, corresponding to a wavelength of 47 nm. This method of high-harmonic generation that requires no extra cavities, eliminate the complex and expensive amplifiers and provide the opportunity to perform HHG experiments at megahertz repetition rates.

To understand the mechanism of the plasmon field-enhanced HHG, we consider a bow-tie-shaped nanostructure irradiated by a femtosecond laser pulse with a low intensity. The positive charges are redistributed around one apex and negative charges around the other one; therefore a hot spot of an intense field is generated. As a result, when a gas jet of argon is injected through a nozzle to this hot spot to provide a surface density, an enhanced HHG spectrum is efficiently generated.

For consideration the presence effect of the metal nanostructure, we describe HHG in the framework of an extended electric field model, i.e., spatiotemporal profile. This inhomogeneity of the field in the hot spot can be considered as perturbative and linear with respect to position. In fact, the above approximation corresponds to the first term of the actual field of a plasmonic nanostructure with spherical shape[14,15].

For nonhomogeneous driving field, up till now, different analytical and numerical approaches have been employed to calculate the HHG (see e.g.[16,17] and references there in), while only few theoretical approaches have been developed to generate a wide supercontinuum and isolated attosecond pulse[18,19].

We adopted pulse chirping approach in the present investigation, to achieve cutoff harmonic extension and produce a wide supercontinuum that enables the generation of attosecond pulse from a modest femtosecond oscillator through field enhancement around the bow-tie-shaped nanostructure.

Furthermore, we present a semi-classical simulation of the HHG process and time-frequency method to analyze these results. This paper is organized as follows. The simulation methods are described in section 2. The influence of time dependent carrier-envelope-phase effects on cutoff position in the presence of the

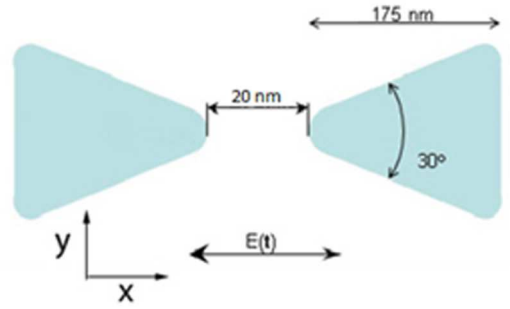

Fig. 1 Geometrical conditions for a single bow-tie element. The polarization direction of the incident pulse is parallel to the x direction.

field inhomogeneity presented and discussed in section 3. Unless otherwise stated, atomic units are used throughout this paper.

Theoretical methods

We consider a hydrogen atom exposed to a linearly polarized (along the z axis) laser field using the single-electron approximation. The one dimensional (1D) time-dependent Schrodinger equation (TDSE) is

$$i\frac{\partial\psi(x,t)}{\partial t}=\hat{\mathrm{H}}(t)\psi(x,t)=\left(-\frac{1}{2}\frac{\partial^2}{\partial x^2}+V_a(x)+V_{\mathrm{int}}(x,t)\right)\psi(x,t), \quad (1)$$

where $V_a(x)=-\dfrac{1}{\sqrt{x^2+2}}$ is the "soft-core" potential, $V_{\mathrm{int}}(x,t)$ represents the interaction term. We model the interaction term $V_{\mathrm{int}}(x,t)$ by[18]

$$V_{\mathrm{int}}(x,t)=xE(z,t), \quad (2)$$

where $E(x,t)=E_0 f(t)\cos(\omega_0 t+\varphi(t))g(x)$ is the spatially inhomogeneous laser field. E_0 is the amplitude, $f(t)$ is the pulse envelope, ω_0 is the frequency and $\varphi(t)=-\alpha\tanh(t/\tau_0)$ is the considered time-dependent carrier-envelope phase (CEP) of the laser field[20]. Here α is the chirp parameter of the pulse (in rad), τ_0 is the parameter of controlling the steepness of the chirped function. We assume that the time profile of $f(t)$ is given by

$$f(t)=\exp(-4Ln2(t^2/\tau^2)), \quad (3)$$

where τ is the pulse duration at full width of half maximum (FWHM). The $g(x)$ function represents the functional form of the nonhomogeneous field which created in the vicinity of metallic nanostructures. Structure and parameters of the studied bow-tie shape of the nanostructure elements — a pair of triangular patches placed apex to apex with a small gap between them — are shown in Fig. 1[9]. As illustrated in this figure, the bow-tie shape is characterized by three geometrical parameters, the angle (30^0), gap (20 nm) and height (175 nm). For these plasmonic enhanced fields, to a first approximation one can employ

$$g(x)\approx(1+\beta x). \quad (4)$$

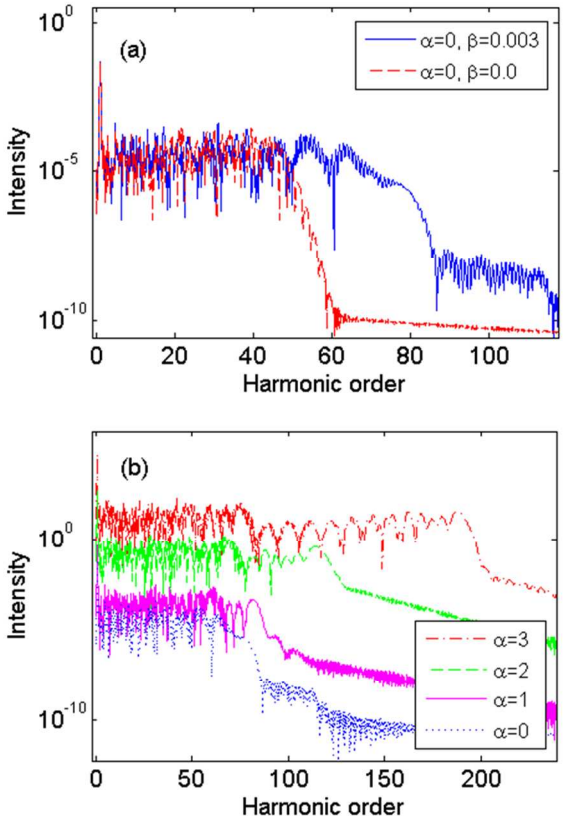

Fig. 2 Photoelectron spectra for a hydrogen atom, (a) Dashed red curve: $\beta=0$ (homogeneous case), Solid blue curve: $\beta=0.003$ (nonhomogeneous). (b) Different values of the chirped parameter for the inhomogeneity parameter $\beta=0.003$, as denoted in the legend. Here, the lines are too close to distinguish, so the HHG spectra are shifted by 2 gradually. The laser wavelength is $\lambda=800nm$ and the intensity is $I=3\times10^{14}W/cm^2$.

The parameter β characterizes the inhomogeneity region which could be related to the gap size of the bow-tie nanostructure of Ref.[9] and its unit is in the reciprocal length.

In our scheme, the parameter β can be extracted by inspecting the HHG spectra obtained from the 1D-TDSE. The procedure would be as follows:

(i) for a given cutoff order from measured spectrum of generated high harmonics in the bow-tie nanostructure of Ref.[9], make a first estimation of the laser intensity (or E_0) using Eq.(4), i.e. using an homogeneous electric field ($\beta=0$);

(ii) introduce a small value of β and solve the 1D-TDSE by reducing the laser intensity (in general smaller intensity values will be needed) till the same cutoff prescribed in (i) is reached;

(iii) record the values of β and E_0 to establish if they are consistent with the geometry of the nanostructure and the experimental conditions.

For the problem we study in this paper, this is a good approximation as far as strong field is concern since the excursion

of the electron is very small and it sees a liner inhomogeneous field.

Equation (1) is solved accurately and efficiently by means of the split-operator method[21]. Once the time evolution of the wave function $\psi(x,t)$ is calculated, the time-dependent induced dipole acceleration can be given by means of the following commutator relation

$$a(t)=\frac{d^2<x>}{dt^2}=-<\psi(x,t)|\hat{H}(t),[\hat{H}(t),x]|\psi(x,t)>\ , \qquad (5)$$

and the HHG power spectrum can be determined, which is proportional to the modulus squared of the Fourier transform of $a(t)$. It is given by

$$P(\omega)=\left|\frac{1}{\sqrt{2\pi}}\int_{-\infty}^{\infty}dte^{-i\omega t}a(t)\right|^2 . \qquad (6)$$

By superposing several harmonics, an ultra-short pulse can be generated,

$$I_{ultra}(t)=\left|\sum_q a_q e^{-iq\omega t}\right|^2 , \qquad (7)$$

where $a_q=\int a(t)e^{-iq\omega t}dt$.

To understand the physics behind the dynamic of HHG, the three-step simulation are performed[8].

If an electron is ionized at t_i from the parent ion $x(t_i)=0$ with the velocity $\dot{x}(t_i)=0$, the corresponding emission time t_f ($x(t_f)=0$) can be obtained by solving the following Newton equation

$$\ddot{x}(t)=-\frac{dV_{\text{int}}(x,t)}{dx} . \qquad (8)$$

Thus, the kinetic energy E_k of the returning electron is expressed as

$$[E_k=\frac{1}{2}\int_{t_i}^{t_r}E(t)]^2 . \qquad (9)$$

By solving equations (8) and (9), we can investigate the electronic dynamics of the HHG process in the laser field.

Results and discussion

We performed the calculations with few-cycle chirped pulses corresponding to pulse duration of 10 fs full width at half maximum. The pulse intensity is $3\times10^{14}W/cm^2$ and the central wavelength is 800nm. We calculate both photoelectron spectra $P(\omega)$ and energy distributions of one-dimensional electron in order to investigate the influence of the field inhomogeneities and the sensitivity of these two quantities to the laser CEP parameter.

For the cases of $\beta=0$ (homogeneous field, i.e., in absence of the typical metallic nanostructure) and $\beta=0.003$ (inhomogeneous field, i.e., in presence of the typical metallic nanostructure)), the harmonic spectra are shown by the red dashed and blue solid curves in Fig. 2a, respectively. As shown by the red dashed curve in Fig. 2a, the spectrum cutoff is at the 47th harmonic order, which corresponds to a photon of 73 eV and the harmonic is modulated. For the blue solid curve, the spectrum cutoff is

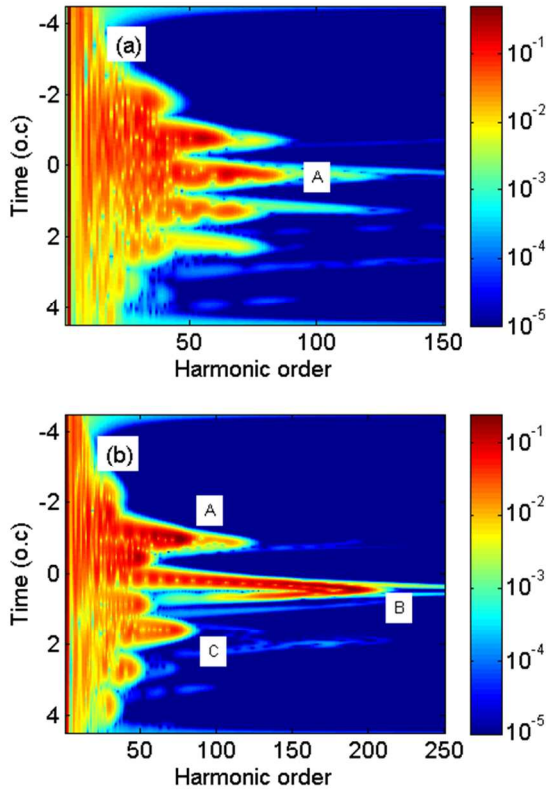

Fig. 3 Time-frequency distribution of the HHG spectrum of hydrogen with two different α parameters (a): $\alpha=0\,rad$, (b) $\alpha=3\,rad$. β is set to 0.003.

significantly expanded to the 78th harmonic order, which corresponds to a photon of 121eV energy and the overall spectral structure is irregular for the harmonics bellow 72nd order, and is smooth from 73rd to 78th order. This smooth behavior lies in the fact that a single radiation burst is produced, i.e. during the process of HHG the cutoff harmonic photons are produced only once.

Furthermore, from the physical view, due to inhomogeneity of electric field the photoelectrons that are released around the maximum of the electric field are more reaccelerated and acquire additional kinetic energy in the continuum (compared with the homogenous driving field) before recombination with parent ions. Therefore, the harmonic cutoff is significantly increased. Also, according to Fig. 2a, the spectrum intensities below the 47th harmonic order almost the same for both cases.

Thus, the characteristic HHG spectrum, with well-developed plateau and cutoff is clearly visible for this local field enhancement induced by resonant plasmons within a metallic nanostructure.

In order to obtain the wide and continuous HHG spectra, we investigate the chirped inhomogeneous field. For chosen values of the laser pulse parameters, $\tau_0=200$ and $\beta=0.003$, HHG spectra when the chirp parameter α is 0, 1, 2 and 3 rad are

plotted by the blue dashed, magenta solid, green dashed and red dash-dotted lines, respectively, in Fig. 2b. With the increase of the chirp parameter α from 0 to 3 rad, the maximum cutoff energy is notably extended from 78th to 188th harmonic order, resulting in a continuum (i.e., the region with low modulation between the maximum cutoff energy and the second maximum cutoff energy) with a bandwidth of about 8 to 104 eV. Thus the bandwidth of the continuum spectrum for adding the frequency chirp to in inhomogeneous field is much broader than that in the chirp-free inhomogeneous field alone.

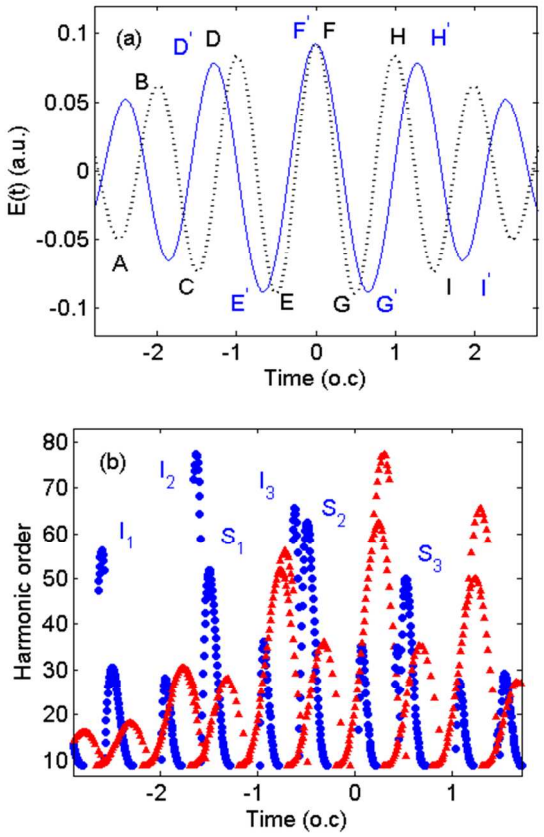

Fig. 4a The profiles of the laser fields at $\alpha = 0 rad$ (black dotted curve), i.e., the chirp-free pulse and $\alpha = 3 rad$ (blue solid curve), i.e., the chirped pulse. τ_0 is set to 200. (b) Harmonic order as a function of the ionization time (the blue circular curve) and recombination time (the red trigonal curve) for the $\alpha = 0 rad$ (chirp-free pulse) and $\beta = 0.003$. o.c. denotes optical cycle.

To well understand the spectral structure shown by the dotted blue and dash-dotted red curves in Fig. 2b, we investigate the emission time of the harmonics by using the time-frequency analysis method[22]. Fig. 3a shows the time-frequency distributions of the HHG for the case $\alpha = 0$ rad . The calculated results show that there are multi peaks contributing to the HHG. For the harmonics bellow about 72th order, there are two dominant quantum electron paths (so-called short and long paths) with different emission times contributing to each harmonic in the range of each peak, and the upside and underside of the peak correspond to the short and long paths, respectively. These harmonics are not emitted in phase and the contributions of these two paths are approximately equal. As a result of the interference, the modulation was extremely strong. A main peak (labeled as A) where the harmonic orders are greater than about 72nd overtops all the adjacent Peaks. In this case, two dominant electron paths are jointed together and constitute a regular modulation from 73rd to 78th harmonic order. For the case of the chirped laser pulse ($\alpha = 3 rad$), time–frequency distribution is shown in Fig.

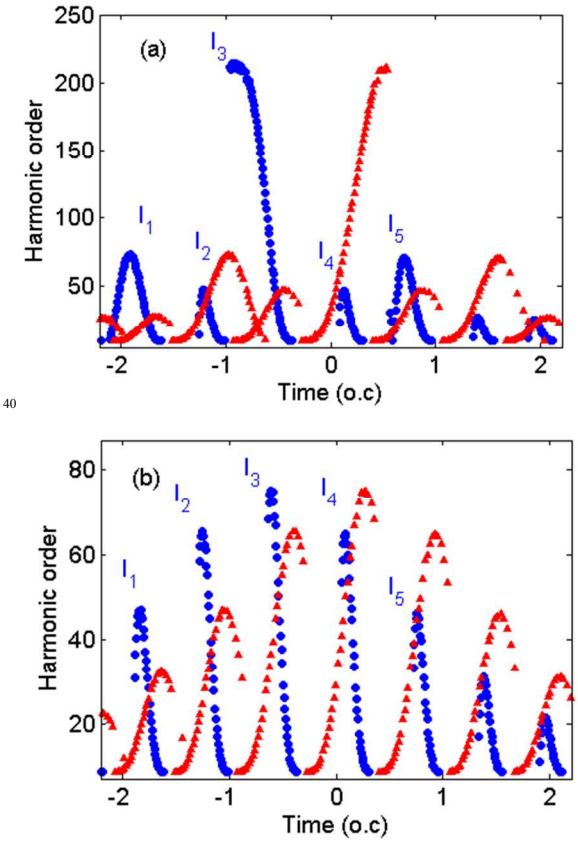

Fig. 5 Harmonic order as a function of the ionization and recombination times for the following values of the parameter: (a) $\alpha = 3 rad$ and $\beta = 0.003$, and (b) $\alpha = 3 rad$ and $\beta = 0$.

3b. As shown in figure, there are three main peaks contributing to the harmonic generation from 72nd to 215th order, which are labeled as A, B, and C, respectively. The maximum harmonic orders of A, B, and C are about 76th, 112nd, and 127th, respectively. For the harmonics above 76th order (in the peak A), there are two dominant electron paths. The intensity contribution of the long paths is lower than that of the short paths. So, spectrum is smooth and regularly modulated for the harmonics through the second plateau to the cutoff.

Furthermore, the intensity of A is the strongest in the three peaks, and the intensity of C is the weakest, resulting in a double-plateau structure in the spectrum shown by the dash-dotted red curve in Fig. 2b.

To explore the underlying mechanism of the HHG chirped, Figs. 4 and 5 illustrate the semi-classical electronic dynamics of the HHG process in our inhomogenous region pulse with two values

of the chirp parameter $\alpha = 0\,rad$ and $\alpha = 3\,rad$. Fig. 4a shows the electric field of the chirp-free field (black dotted curve) and Fig. 4b shows the corresponding dependence of the harmonic order on the ionization (blue circles) and emission times (red triangles). It is noted that the harmonic order is given by the following formula:

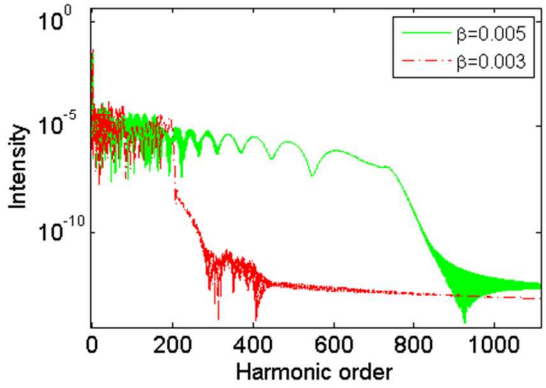

Fig. 6 Photoelectron spectra for a hydrogen atom: Dotted-Dashed red curve: $\beta = 0.003$, Solid green curve: $\beta = 0.005$. α is set to 3rad.

$$(I_p + E_k), \qquad (10)$$

where I_p is the ionization potential and E_k is the kinetic energy of the electron quivering in the laser field (Equation (9)).

Obviously, in cutoff region, there are three main peaks with internal peak on the ionization and emission energy map for the $\alpha = 0\,rad$ case (Fig. 4b), which should be caused by three events of the HHG process, i.e., ionization, acceleration and recombination[11].

As shown in Fig. 4b, three exterior peaks, I_1, I_2 and I_3 caused by three events of the process labeled as A-BCD-E, C-DEF-G, and E-FGH-I in the profile of the driving field in Fig. 4a. Similarly, three interior peaks, S_1, S_2 and S_3 caused by processes labeled as $D'E'F'$, $E'F'G'$, and $F'G'H'$ in Fig. 4a. The time of electron flight for exterior peaks is nearly two times longer than interior peaks. All of these observations can be as a result of field inhomogeneity.

Moreover, the highest emission energy of the peak I_2 is 78th harmonic, corresponding to the cutoff energy at 121eV. These results shown in Fig. 4b are in agreement with above mentioned quantum analysis and numerical TDSE calculation.

In the $\alpha = 3\,rad$ case (Fig. 5a), there are also five main peaks I_1, I_2, I_3, I_4 and I_5 (ionization peaks), but the highest emission energy of the peak I_3 is determined by the $E'F'G'$ events has been clearly enhanced to 215th harmonic order (i.e., 333eV).

By introducing the chirp to the driving field, although the strength of the amplitude (peak F or F') remains approximately unchanged but the $E'F'G'$ events has been clearly broadened; hence, the ionized electron must obtain much more time at presence of the reversed electric field, which is responsible for the extension of the cutoff energy.

In addition, as seen in Fig. 5a, the electron trajectories of the HHG can be significantly modulated, as, the short trajectories can be easily selected to contribute to the harmonics above 112nd order. Thus, the modulations in this second plateau can be reduced by adding a frequency chirp to laser field.

To investigate the effect of inhomogeneity on the electron trajectories of the HHG correspond to chirped driving field, the harmonic emission map for homogenous field is analyzed in terms of semi-classical electronic analysis.

We can see that Fig. 5b exhibits distinct features compared with the inhomogeneous field (Fig. 5a).

As shown in Fig. 5b, there are five main ionization peaks (labeled as I_1, I_2, I_3, I_4 and I_5) corresponding to the higher-order harmonic and the highest emission energy of the peak I_3 is 75th harmonic order.

In comparison with the homogeneous field (Fig. 5b), the peaks, I_1, I_3 and I_5 are increased (in Fig. 5a), while the other peaks I_2 and I_4 are decreased. On the other hand, the broken inversion symmetry as an effect of the field inhomogeneity, led to a dramatic increase (and decrease) in the positive (and negative) field which felt by the electron. Similarly to the case of the chirp-free in homogenous field (Fig. 4b), the agreement of the semi-classical and the quantum results are excellent.

In Fig. 6, the dependence of harmonic orders on inhomogeneity parameter is investigated for chirped driving pulse $\alpha = 3\,rad$.

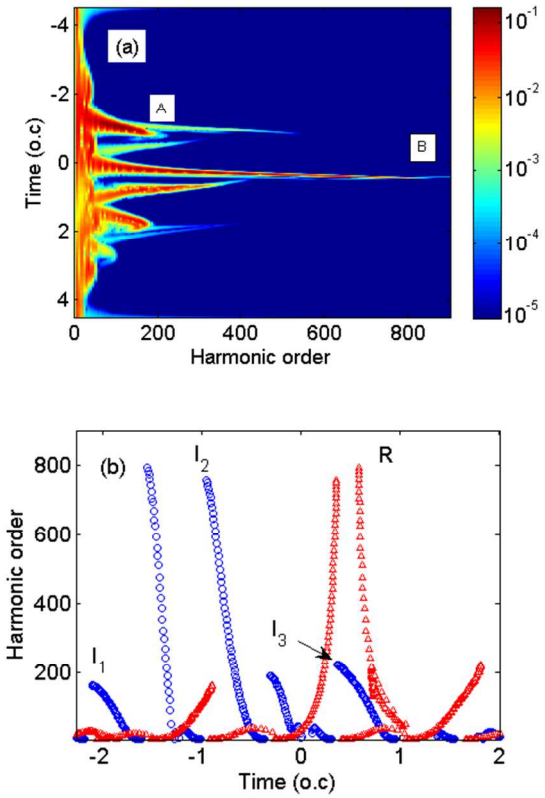

Fig. 7a Time-frequency distribution of the HHG spectrum for the following values of the parameter: $\alpha = 3\,rad$ and $\beta = 0.005$, (b) The corresponding time–frequency distribution harmonic order as a function of the ionization and recombination times.

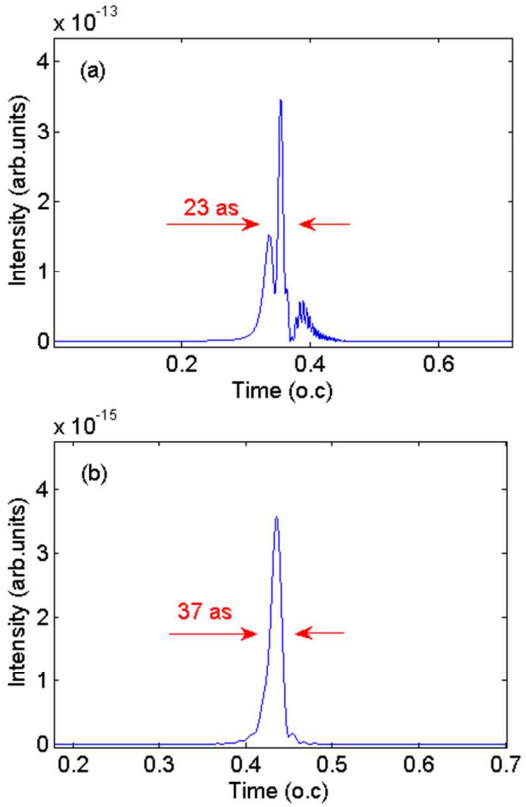

Fig. 8 Temporal variation of the attosecond pulses generated from hydrogen atoms. (a) The harmonics are chosen from the 420th to 780th orders; (b) from the 700th to 780th orders. β and α are set to 0.005 and 3rad, respectively.

With the increase of the inhomogeneity parameter, the position of the cutoff moves from 215th to 740th order and produces a wide supercontinuum with the width of 601 eV (388). Moreover, the corresponding time-frequency distribution is shown in Fig. 7a. One can see that, for harmonics from the 180th to 352nd order, both the long- and short-trajectory electrons emit rapidly and near this cutoff region (the 352nd-order harmonic), the corresponding radiations split. From the 352nd to 740th harmonics, there is a narrow short-path burst with strong intensity. In this case, the long electron path is completely suppressed and the plateau region is further extended in comparison with the Fig. 3b. Therefore, one can see from the solid green curve of Fig. 6 that the spectral profile of the harmonics between 352nd and 740th order are much smoother than that of harmonics between 352nd and 180th order. Indeed, from the time-frequency profile of Figs. 3b and 7a and the harmonic spectrum of Fig. 6, we can see that the modulation of high harmonics for the $\beta = 0.005$ case (the harmonics between 352nd and 740th order) is evidently smaller in comparison with the $\beta = 0.003$ case (the harmonics above 75th).

This is proof of a strong quantum path selection and is the key idea in generating isolated attosecond pulses. These results are in accordance with the results of the three-step model shown in Fig. 7b. As shown in Fig. 7b, there are three dominant ionization peaks (labeled as I_1, I_2 and I_3) corresponding to the harmonic generation. The highest harmonic energy of the peak I_2 is 740th harmonic, corresponding to the cutoff energy at 1147 eV. In fact, after the electrons are ionized, the higher the strength of the reversed inhomogeneous field is, the higher kinetic energy the ionized electrons obtain from the driving laser field. Thus the cutoff energy difference between the two peaks (I_1 and I_2 in Fig. 7b corresponding to two main peaks marked as A and B in Fig. 7a) is much larger than that in Fig. 5a (i.e., I_1 and I_3).

Additionally, for the harmonic photons with order higher than 230, the contribution of the long trajectory has been obviously suppressed; only the short trajectory are kept down. As shown in figure, the electrons at the radiation burst R ionized from −1.55 to −1.39 o.c. contribute to the harmonic generation from 794th to 350th order. From Fig.4a, one can see that the strength of the driving field is negligible at this time interval. Therefore, the electron which ionized at this time interval doesn't play any role in harmonic generation from 794th to 350th order, as observed in Fig. 7a. Therefore, a wide supercontinuum is formed, which is advantageous to obtain an isolated attosecond pulse. Finally, Figs. 8a and b show the temporal profiles of the attosecond pulses generated from the supercontinuum by the $\beta = 0.005$ case in Fig. 6. In Fig. 8a, by superposing the 420th to the 780th harmonic order, an isolated 23-as pulse with several small satellites can be achieved without any phase compensation. By properly superposing the 700th to the 780th harmonic order, the satellite pulses have been suppressed, and a clean isolated 23-as pulse can be achieved, as shown in Fig. 8b.

Conclusions

We have numerically investigated the high-order harmonic generation and harmonic-cutoff extension phenomenon controlled by a few-cycle chirped laser pulse by means of plasmonic field enhancement in metallic nanostructures. For modelling the metallic nanostructures, we considered a linear term to the approximated inhomogenous field. Our calculations showed that the field inhomogeneity plays a critical role in systematic increase in the cutoff position.

Based on the classical trajectory simulation and fully quantum investigation, with the introduction of chirping and plasmonic field enhancing, the electron trajectories are fully modulated and the wide supercontinuum can be generated. Our procedure can be introduced as a suitable source to generate a single radiation with a sub-30-as duration.

Notes and references

[a] *Department of Physics, Faculty of Science, Guilan University, Rasht, Iran, Full Postal code 4193833697. Fax: +981313220066; Tel: +98 1313243630;*
E-mail: hd_hekmat@yahoo.com

1 P. Vasa, C. Ropers, R. Pomraenke, & C. Lienau, *Laser Photon. Rev.* 2009, **3**, 483.
2 M. I. Stockman, *New J. Phys*. 2008, **10**, 025031.

3 H. Fischer, & O. J. F. *Opt. Express*, 2008, **16**, 9144.

4 D. A. Genov, V. M. Sarychev, V. M. Shalaev, & A. Wei, *Nano Lett*. 2004, **4**, 153.

5 J. Merlein, et al. *Nature Photon*. 2008, **2**, 230.

6 D. P. Fromm, A. Sundaramurthy, P. J. Schuck, G. Kino, & W. E. Moerner, *Nano Lett*. 2004, **4**, 957.

7 K. Li, M. I. Stockman, & D. J. Bergman, *Phys. Rev. Lett.* 2003, **91**, 227402.

8 T. Hanke, et al. Phys. Rev. Lett. 2009, **103**, 257404.

9 S. Kim, J. Jin, Y.-J. Kim, I.-Y. Park, Y. Kim, and S.-W. Kim, *Nature*, 2008, **453**, 757.

10 I.-Y. Park, S. Kim, J. Choi, D.-H. L. Y.-J. Kim, M. F. Kling, M. I. Stockman, and S.-W. Kim, *Nat. Phot.* 2011, **5**, 677.

11 P. B. Corkum, *Phys. Rev. Lett.* 1994, **71**, 1993.

12 M. R. Roth, C. N. Panoiu, M. M. Adams, & M. R. Jr. Osgood, *Opt. Express*, 2006, **14**, 2921.

13 L. J. Bohn, J. D. Nesbitt, & A. Gallagher, *J. Opt. Soc. Am. A*, 2001, **18**, 2998.

14 F. Sußmann and M. F. Kling, *Proc. SPIE 8096, 80961C* 2011.

15 T. Shaaran, M. F. Ciappina, and M. Lewenstein. *Phy Rev A*, 2012, **86**, 023408.

16 P. Saileres, A. L'Huillier, P. Antoine, and M. Lewenstein, Advances of Atomic and Molecular Physics, edited by B. Bederson and H.Walther (*Academic Press, New York*, 1999).

17 A. L'Huillier and M. Lewenstein, Springer Series in Optical Sciences, edited by T. Brabec (*Springer, Berlin*, 2008).

18 A. Husakou, S.-J. Im, and J. Herrmann, *Phys. Rev. A*, 2011, **83**, 043839.

19 I. Yavuz, E. A. Bleda, Z. Altun, and T. Topcu, *Phys. Rev. A*, 2012, **85**, 013416.

20 J.J. Carrera, S.I. Chu, *Phys. Rev. A*, 2007, **75**, 033807.

21 M. D. Feit, J. A. Fleck, and A. Steiger, *J. Comput. Phys.* 1982, **47**, 412.

22 P. Antoine and B. Piraux, *Phys. Rev. A*, 1995, **51**, R1750.

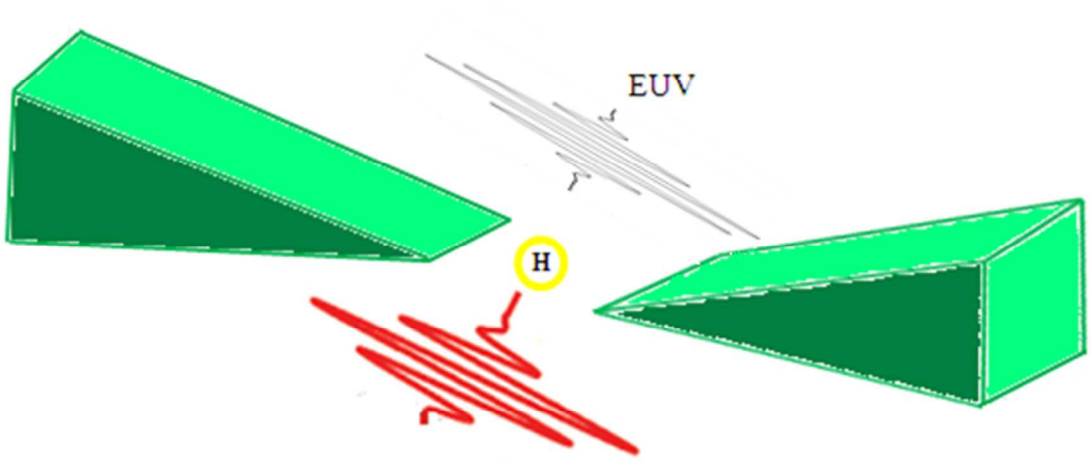

By using suitable chirping field, an ultrashort pulse was obtained in the vicinity of metal nanostructure.